Engineering Structures 140 (2017) 151–163

Contents lists available at ScienceDirect

Engineering Structures

journal homepage: www.elsevier.com/locate/engstruct

Behavior of RC beams strengthened with strain hardening cementitious composites (SHCC) subjected to monotonic and repeated loads

Abd El-Hakim Khalil, Emad Etman, Ahmed Atta *, Mohamed Essam

Faculty of Engineering, Tanta University, Tanta, Egypt

ARTICLE INFO

Article history:
Received 29 June 2016
Revised 18 February 2017
Accepted 19 February 2017
Available online 9 March 2017

Keywords:
RC beams
Strengthening
UHP-SHCC
Ductility
Repeated load
Dissipated energy
Stiffness degradation

ABSTRACT

Ultra High Performance Strain Hardening Cementitious Composites (UHP-SHCC) is a newly developed construction material, has large advantages on large strain capacity as well as high compressive and tensile strength, which is useful for strengthening or repair concrete members. However, some important obstacles need to be studied, such as the strain localization occurs in the UHP-SHCC strengthening layer around the substrate concrete cracks, which severely limits the ductility of the strengthened beam subjected to monotonic and repeated loads. In the present study, ten specimens were tested experimentally, which divided into two major groups, each group contains five specimens, one as a control and four strengthened with constant UHP-SHCC layer thickness having variable reinforcement ratios embedded in the middle of the strengthening layer. Two types of loading were applied; Monotonic loading for the first group and short time repeated loading for the second group. The recorded tests showed that use additional reinforcement embedded in the strengthening layer for beams strengthened with UHP-SHCC become sufficient at certain limit to eliminate the observed early strain localization and to gain adequate ductility under both monotonic and repeated loading. Another important conclusion is the strengthening of RC structures using an unreinforced UHP-SHCC layer may lead to a brittle failure especially in case of repeated loading.

© 2017 Elsevier Ltd. All rights reserved.

1. Introduction

In recent years, in order to overcome the various shortages of material developed for repairing or retrofitting, High performance cementitious materials are developed, which can be called as High performance Fiber-reinforced Cementitious Composites (HPFRCC) [6]. HPFRCC are normally adopted due to some advantages, such as strain-hardening Behavior. One typical type of HPFRCC is strain hardening cementitious composites (SHCC) with higher ductility, which is an attractive material for surface repairing and strengthening. The typical type of SHCC is engineered cementitious composites (ECC) [12,13,15,16,14]. ECC can exhibit tensile strain capacity more than 1 or 2%. However, the durability of ECC may be decreased due to the low performance of matrix [17]. Besides, the compressive strength of ECC is limited. Another typical HPFRCC is Ultra High Performance Fiber-reinforced Concretes (UHPFRC), which exhibits strain-hardening under uniaxial tension and very high strength. However, it also has a limitation of strain capacity.

In order to improve the performance of ordinary HPFRCC, a new type of HPFRCC material, called as Ultra High Performance Strain Hardening Cementitious Composites (UHP-SHCC), is developed by Kamal et al. [7], with special objective of high tensile and compressive strength, large strain capacity, high workability, easy processing using conventional equipment, and lower fiber volume fraction [8,9]. Fig. 1 shows the target of UHP-SHCC [10], which has relatively higher hardening strain compared with ordinary UHPFRC, and relatively higher stress than ordinary SHCC. In addition, UHP-SHCC considered a perfect protective material against corrosion [3]. Although having the excellent properties, Ultra High Performance Strain Hardening Cementitious Composites (UHP-SHCC) is not widely adopted in construction until now. Civil engineers seem to lack the necessary innovative spirit to apply this new type of materials in repair or strengthening concrete structures. They tend to adopt traditional material for repair or strengthening damaged or aged concrete structures such as steel plates. On the other hand, one of the primary obstacles preventing the widespread use of UHP-SHCC is the early strain localization occurred in the strengthening layer, therefore [5] presented the ductility behavior in tests on reinforced concrete beams that were strengthened in flexure with lightly steel-reinforced SHCC layer (0.3% and 0.6% steel reinforcement ratio). It has been found that the combination of the SHCC and a small amount of steel reinforcement helps develop higher strain in the SHCC strengthening

* Corresponding author.
E-mail address: Drahmedatta2003@yahoo.com (A. Atta).

http://dx.doi.org/10.1016/j.engstruct.2017.02.049
0141-0296/© 2017 Elsevier Ltd. All rights reserved.

Notations

b	Width of cross section [mm]
t	Total depth of cross section [mm]
d′	Distance from extreme compression fiber to compression reinforcement [mm]
d_s	Distance from extreme compression fiber to center line of main reinforcement in the tension side [mm]
d_{UHP}	Distance from extreme compression fiber to center line of UHP-SHCC strengthening layer [mm]
t_{UHP}	Thickness of UHP-SHCC strengthening layer [mm]
c	Distance from extreme compression fiber to the neutral axis [mm]
λ	Ratio of the depth of the equivalent rectangular stress block to the depth of the neutral axis [---]
f_{cu}	The characteristic compression strength of concrete [MPa]
f'_s	The actual stress of compression reinforcement [MPa]
f_s	The actual stress of tension reinforcement [MPa]
f_{UHP}	The actual tensile strength of UHP-SHCC layer [MPa]
$f_{s,add}$	The actual stress of additional reinforcement embedded in UHP-SHCC layer [MPa]
ε_{cu}	The ultimate compressive strain of concrete [---]
C'_s	The compression force for compression reinforcement [N]
T_s	The tension force for tension reinforcement [N]
T_{UHP}	The tension force for UHP-SHCC layer [N]
$T_{s,add}$	The tension force for additional reinforcement embedded in UHP-SHCC layer [N]
C_c	The compression force for concrete block [N]
A'_s	The area of compression reinforcement cross section [mm^2]
A_s	The area of tension reinforcement cross section [mm^2]
A_{UHP}	The area of UHP-SHCC layer cross section [mm^2]
$A_{s,add}$	The area of additional reinforcement embedded in UHP-SHCC layer cross section [mm^2]
E_s	Modulus of elasticity of all reinforcement bars [MPa]
E_{UHP}	Modulus of elasticity of UHP-SHCC layer [MPa]

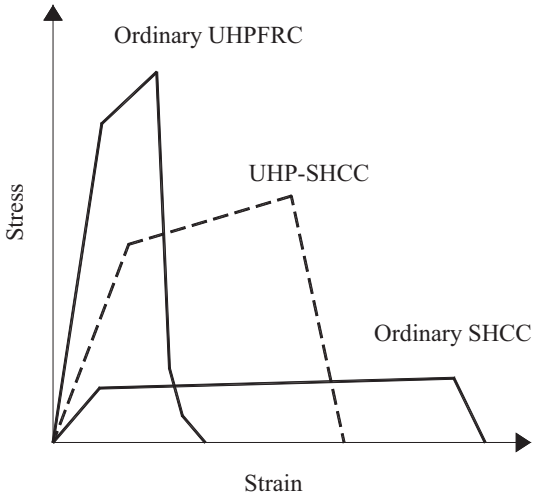


Fig. 1. Target of UHP-SHCC.

layer at ultimate load and eliminates the observed early strain localization.

This study concerned on determining the sufficient amount of reinforcement ratio used in UHP-SHCC layer to get the most possible benefit from using this material as a strengthening layer. Although, since the appearance of UHP-SHCC, it has been an important subject of academic research, mostly focused on understanding the material microstructure and the ductility enhancement under ordinary monotonic loading. However, for design purposes, its structural behavior under repeated loading needs to be thoroughly understood.

2. Experimental program

2.1. Material properties

The mix proportions of the UHP-SHCC used as a strengthening material in this study are listed in Table 1. Water to binder ratio (W/B) was 0.20. Low heat Portland cement (density: 3.14 g/cm^3) was used, and 15% of the design cement content was replaced by silica fume. Quartz sand with diameter less than 0.5 mm was used as a fine aggregate. High strength polyethylene (PE) fiber was chosen for UHP-SHCC and its volume in mix was 2%. The diameter and length of the PE fibers were 0.012 mm and 6 mm, respectively. The tensile behavior of the used UHP-SHCC was characterized by testing of three large size specimens with different embedded reinforcement ratio, as shown in Table 2, (tested cross-section: 50 × 200 mm) in uniaxial tensile test. Fig. 2 shows specimens details and test setup. The averaged tensile strength and ultimate tensile strain (strain at ultimate load) of the reinforced UHP-SHCC without the contribution of embedded reinforcement at the age of 28 days were determined to be 6.5 MPa and 0.45% respectively. Fig. 3 shows the crack pattern of specimens at failure. Fig. 4 shows the stress–strain relationship measured from the uniaxial tensile tests. To characterize the compressive properties of the used UHP-SHCC, six cube specimens having a size of 50 mm were tested at the age of 28 days and the averaged compressive strength was determined to be 78.8 MPa. The used ordinary concrete was made from a mix of ordinary Portland cement, natural sand, and gravel with the mixture proportions shown in Table 1. The averaged compressive strength of the used substrate concrete was determined to be 29 MPa based on the compressive test results of six cube specimens having a size of 150 mm. In order to determine the mechanical properties of the used reinforcement, tensile tests were performed on three specimens of each different type of reinforcement. The mean value of tensile yield strength, tensile strength and Young's modulus for the used 6 mm diameter were 290 MPa, 398 MPa and 190 GPa respectively. For the used 10 mm and 8 mm diameters, the mean value of tensile yield strength, tensile strength and Young's modulus were 400 MPa, 683 MPa and 200 GPa respectively.

2.2. Specimen's details

The experimental program divided into two main groups, each group contains five specimens, one control and four strengthened with constant UHP-SHCC layer thickness having variable reinforcement ratios embedded in the middle of the strengthening layer. All the beams had dimensions of 120 mm width, 200 mm height, and 1800 mm length. Two rebars of 10 mm diameter (D10) were used as tension reinforcement for all the beams. Another two rebars of 8 mm diameter (D8) were used as compression reinforcement for all the beams. Stirrups of 8 mm diameter were used and placed,

Table 1
Mix proportions of UHP-SHCC and ordinary concrete.

Material	Unit content (kg/m^3)								
	Water	Cement	Silica fume	Expansion agent	Sand	Coarse aggregate	Super plasticizer	Air reducer	Fiber (6 mm)
UHP-SHCC	290	1243	223	20	149	–	15	2.98	19.5
Ordinary concrete	175	350	–	–	630	1050	–	–	–

Table 2
Description of tested specimens in uniaxial tensile test.

Specimens	Dimensions (mm)	Reinforcement	ρ_s% (Reinforcement ratio)
S_1		–	–
S_2	50x200x900	1 D 6 mm	0.30
S_3		2 D 6 mm	0.60

as shown in Fig. 5, to prevent the shear failure. All beams were designed according to ACI 318M-14 [2] to make sure tension failure collapse. The concrete dimensions and reinforcement details of the tested specimen were shown in Fig. 5. The beams were demoulded at the age of 2 days, and their bottom surface (tension reinforcement side) was washed out using a retarder to obtain a rough surface. Following the wash-out process the specimens were covered with wet towels for additional 26 days. At the age of 28 days, UHP-SHCC strengthening layer was cast with 40 mm thickness in the beams' tension side (rebar side). For the UHP-SHCC-strengthened beams, two beams were strengthened using unreinforced UHP-SHCC layer, whereas six beams were strengthened with steel reinforced UHP-SHCC layer with variable reinforcement ratio according to Table 3.

2.3. Test setup and instrumentations

All the beams were loaded in four-point bending. The load was applied using a hydraulic actuator through a spreader steel beam to the specimen. Each specimen spanned 1500 mm and was loaded symmetrically about its centerline at two points 600 mm apart. A load cell was attached to the loading actuator to record the applied load. One Pi-shaped displacement transducers was bonded to the top concrete surface of each specimen at midspan, to record the compression strain in the extreme concrete fibers. One strain gauge was bonded to each rebar in the tension side at its midspan. During the test, UHP-SHCC strengthening layer's strains were recorded by Pi-shaped displacement transducers with a gauge length of 100 mm applied on layer's bottom side as shown in Fig. 5, whereas an additional Pi-shaped displacement transducers were used to record the substrate concrete strains at concrete-UHP-SHCC layer interface as shown in Fig. 5. Displacements at midspan was measured using Linear Variable Displacement Transducer (LVDT). An automatic data acquisition system was used to monitor loading, displacements and strains. The instrumentation used to monitor the behavior of the beams during testing is shown in Fig. 5.

2.4. Loading protocol

As described before, All specimens divided into two groups. Group (I) contains five specimens subjected to monotonic loading using displacement-control mode at a rate of 0.05 mm/s until failure. Group (II) contains five specimens subjected to four stages of repeated loading then if failure does not occur during these stages, the system applies monotonic loading under load-control at a rate of 0.10 kN/s until failure. Description of repeated loading stages as follows, the system applies 100 cycles of load/unload between specified values of the load range (10–30%, 10–50%, 10–70% and 10–90%) of the expected failure load evaluated from group (I).

3. Test results and discussion

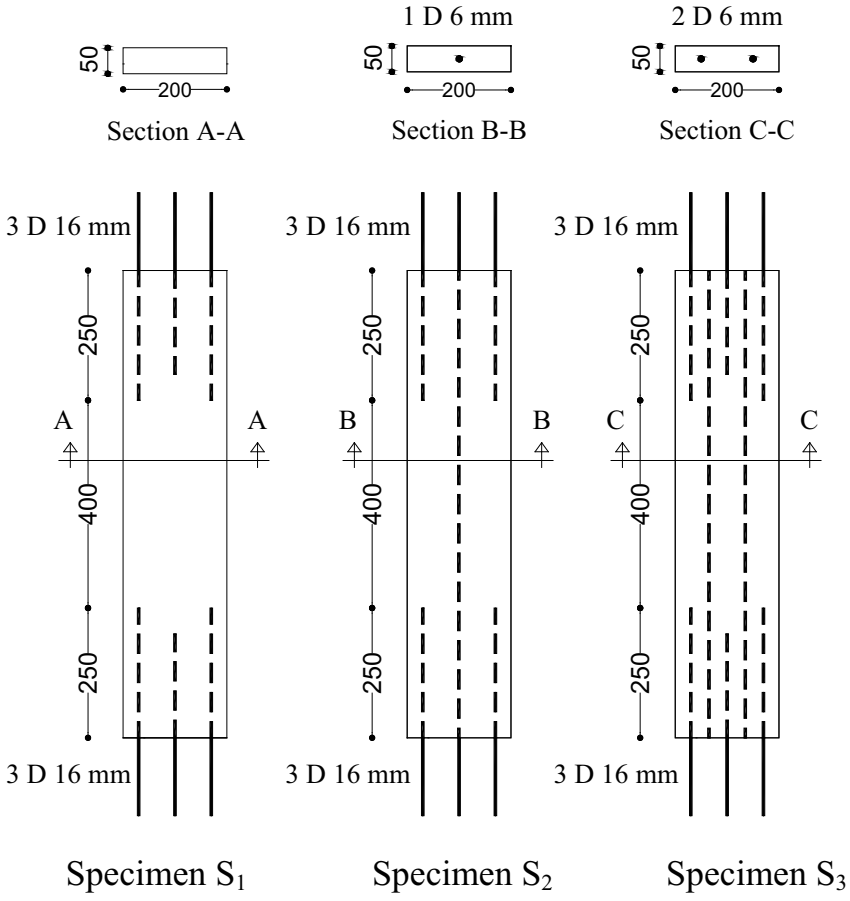
3.1. Loads, cracks pattern and failure modes

For group (I), the control specimen, beam (BSC), was failed as expected in flexure with extensive yielding of the tension steel. The cracks were initiated at the soffit beam section at load 15.2 kN. The failure of this beam started with yielding of tension steel and ended with crushing of concrete at load 53.4 kN in the compression side of the beam, according to strain monitoring realized during the test. For all strengthened beams in group (I), during loading process, flexure cracks started to appear in substrate concrete at the tension side of the beam within the middle third at cracking loads 31.4, 32.0, 32.2 and 32.9 kN for strengthened beams BS0, BS1, BS2 and BS3, respectively. With increase in load the crack started to appear in the strengthening layer and propagated upward in substrate concrete. The beam continued to support the applied load until failure was occurred, at ultimate loads 77.0, 84.0, 94.0 and 103.7 kN for strengthened beams BS0, BS1, BS2 and BS3, respectively. At failure, the strengthening layer was ruptured near the mid span or loading points, after yielding of the reinforcing steel bars and before concrete crushing in the compression zone, according to strain monitoring realized during the test.

For group (II), the control and strengthened specimens had the same failure mode of specimens in group (I), however the failure load was decreased due to the damage level occurred in the specimens under the effect of repeated loading. The load carrying capacity of beams BRC, BR0, BR1, BR2 and BR3 was decreased by 8%, 9%, 7%, 4% and 4%, respectively. Although failure of the beams strengthened using steel reinforced and unreinforced UHP-SHCC layer was by rupture of fibers in UHP-SHCC layer, formation of distributed visible cracks in UHP-SHCC layer for beams strengthened with reinforcement ratio 1.2% and 1.8% made its failure more predictable than other beams as shown in Fig. 6. When 1.2% and 1.8% reinforcement ratio were used there seems to be a delay in the formation of wide cracks in the UHP-SHCC layer, which allows the beam to achieve considerably higher deflection and ultimate loads compared to beams BS0 and BR0. The ultimate loads, the cracking loads, and the yielding loads are shown in Table 4. Experimental results reported in Table 4 indicate an increase of varying degrees in the cracking load for all of the strengthened beams over that of the control beam. This is to be expected, partially because of the stiffening of the beams due to the application of the strengthening layer.

3.2. Load versus deflection response at midspan

Fig. 7 shows the measured load deflection response for beams in group (I). The control beam (BSC) showed the usual elastic and inelastic parts of its deflection behavior and failed, as expected, due to yielding of the tensile steel reinforcement prior to crushing of the concrete at significantly high final deflections than the



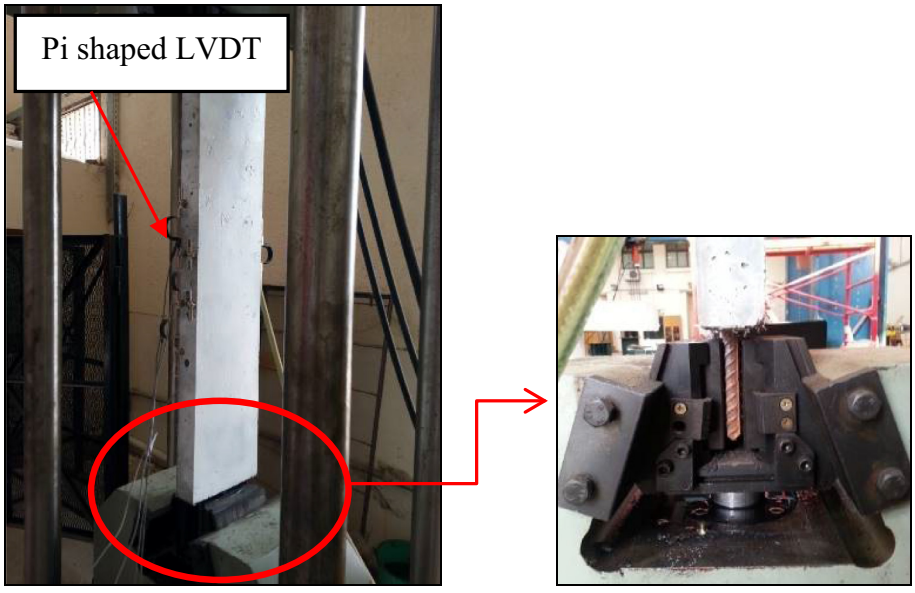


Fig. 2. Uniaxial test setup and specimens details.

UHP-SHCC strengthened beams. The characteristics of the load–deflection behavior of beam BS0 may be summarized as follows. Initially, the behavior is linear up to the cracking load, with cracks appearing near the beam's mid-span the curve begins to deviate from the linear path. After the strengthened beam reaches its maximum load, the load drops rapidly from the peak to a significantly lower load level round the control beam (BSC) capacity due to the localized failure of the strengthening layer which produced by the high strain concentration points in UHP-SHCC layer developed by the cracks in the concrete substrate as discussed before, and then the beam's behavior was controlled by the original steel reinforcement.

Strengthened beams BS1, BS2 and BS3, provided with 0.6%, 1.2% and 1.8% reinforcement ratio respectively, demonstrated the same

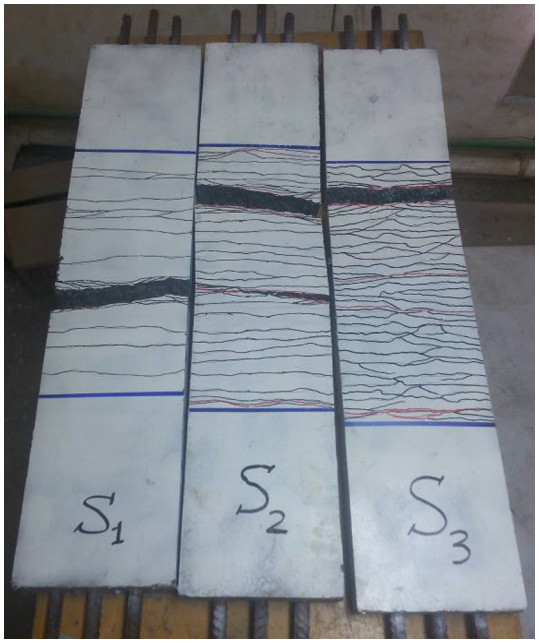


Fig. 3. Cracks pattern for specimens in uniaxial test.

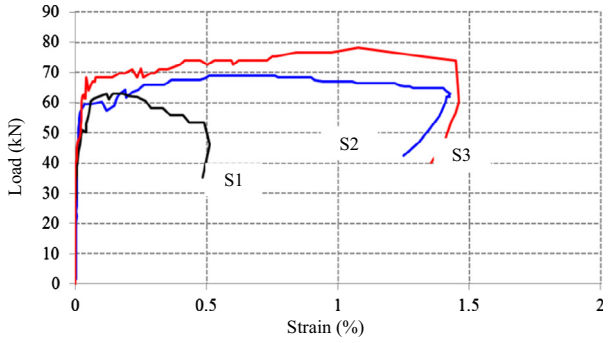


Fig. 4. Load versus tensile strain for tested specimens.

load–deflection response, as beam BS0, up to maximum load. However, after the beams reached their maximum load, as can be seen in Fig. 7, they were able to sustain inelastic deformation prior to collapse, without significant loss in resistance. This might be attributed to a greater resistance to local failure of steel-reinforced UHP-SHCC. In addition, the sustained inelastic deformation was increased by increasing reinforcement ratio. After the strengthened beams reached their maximum load, and contrary to the observed behavior of BS0, the curve demonstrated a softening tail, and the load drops gradually from the peak to a constant load level for each beam. Thereafter, the beams behavior was controlled by the steel reinforcement. Fig. 8 shows the load-deflection hysteresis loops of specimens in group (II). It was observed that the relation was to be linear before cracking stage. After cracking stage, slope of the hysteresis curves (secant stiffness) degrades with increase of load and the failure occurred at loads 49.7, 71.0, 79.0, 91.0 and 100 kN for specimens BRC, BR0, BR1, BR2 and BR3, respectively.

3.3. Cracks behavior

The load-crack width response for all tested specimens in group (I) is shown in Fig. 9. The crack width were measured for all beams at 20 mm from beam soffit in the substrate concrete by using a microscope and taken as the maximum crack within the middle third. It can be seen that cracks were much wider on the control beam, for all loads. The first crack was noticed on the control beam when the applied load reached about 15.2 kN and, nearly the maximum load (53.4 kN), the maximum crack width on the constant moment region was 6.5 mm. Fig. 9 clearly reveals the significant improvement in the UHP-SHCC cracking behavior provided with the proposed steel reinforcement, crack width of the UHP-SHCC strengthened beams BS0, BS1, BS2 and BS3, at about maximum load, reached 1.9, 1.6, 1.25 and 1.2 mm respectively, where 1.2% and 1.8% reinforcement ratio used in strengthening layer succeeded to reduced crack width of the control beam by 82% due to the effect of fiber bridging action in the strengthening layer, which control the cracks width.

The summary of the crack observations, examined immediately before failure, for all of the strengthened specimens is given in Table 4 including the number of the developed cracks in the middle third span at which failure occurred (N), the average of crack spacing (S_{av}) and the maximum of crack spacing (S_{max}), observed in the strengthening layer. It can be clearly seen from the summary of the test results presented in Table 4 that while increasing the reinforcement ratio the averaged crack spacing will gradually be reduced whereas the number of developed cracks will be increased. 0.6% reinforcement ratio enabled beams BS1 and BR1 to develop 46 and 51 cracks, almost twice the number in beams BS0 and BR0, 1.2% and 1.8% reinforcement ratio enabled beams BS2, BS3, BR2 and BR3 to develop 66, 69, 72 and 74 cracks respectively, which consider triple the number developed in BS0 and BR0. From these results we could summarized that increasing the reinforcement ratio in the strengthening layer helps to distribute cracks uniformly and reduce the width of the crack which leads to enhancement in cracks behavior.

In generally, Specimens subjected to repeated loading enabled to develop number of cracks greater than specimens subjected to static load, that may be due to the specimens under repeated loading suffers greater deformation than under static loading as mentioned above, this helps cracks grow and spread under repeated cycles of loading, also the loading and unloading branches of the load deflection curve form a hysteresis loop, the area within this loop represents the irreversible energy of deformation, that is the energy that propagates the cracks. Comparing to the number of cracks developed in specimens under static loading, beams under repeated loading enabled to increase number of cracks by 18%, 11%, 9%, 8% for beams BR0, BR1, BR2 and BR3 respectively.

3.4. Ductility analysis

In strengthening of RC structures with UHP-SHCC it is notable that the increase in strength and stiffness is sometimes attained at the expense of a loss in ductility, or loss of capacity of the structures to deflect inelastically while sustaining a significant percentage of its maximum load. Ductility is an important property for safe design of strengthening of any structural element. As UHP-SHCC strengthening is a relative recent strengthening strategy, understanding the effect of this technique on the ductility of a RC member is crucial. Therefore, the ductility index ($\mu_{\emptyset}$), which expressed as the ratio between the curvature at the ultimate condition ($\emptyset_u$) and curvature at the yield load ($\emptyset_y$), will be the indicator of ductility for group (I). The curvature calculated using the inclination of strain distribution along the depth of the cross section of the beam.

Table 5 lists the values of the ductility index for all beams in group (I). According to the (FIB, 1990) recommendations, the minimum ductility index, in terms of curvature, should be approximately 1.7 and 2.6 for concrete types C35/45 or lower and concrete types higher than C35/45, respectively. The ductility

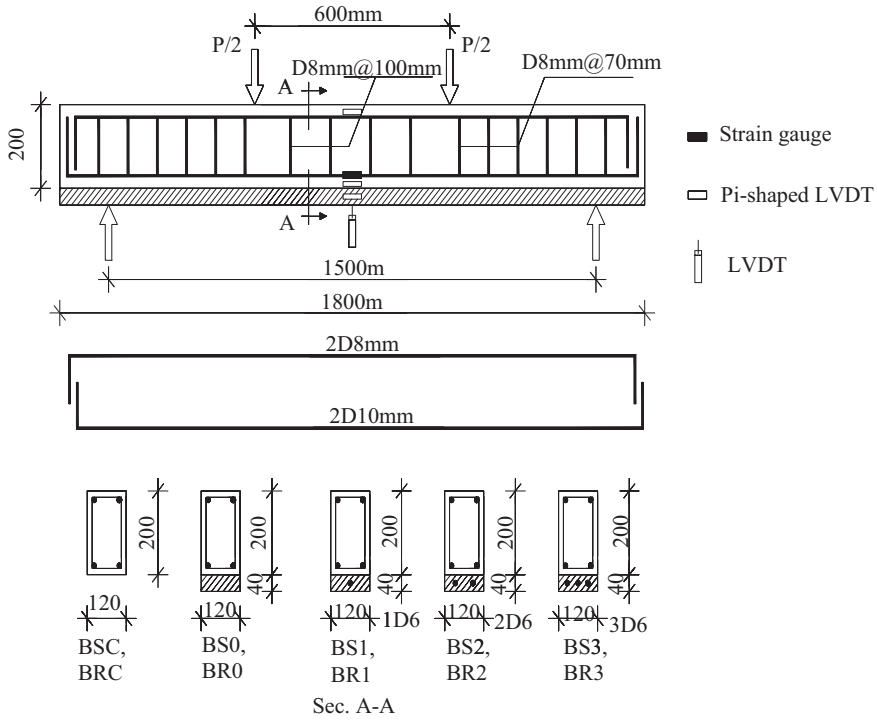


Fig. 5. Test setup and specimens details.

Table 3
Details of tested specimens.

Specimen	Cross section dimension (mm)	Loading type	Thickness of UHP-SHCC layer (mm)	Strengthening layer reinforcement	
				RFT	Ratio%
BSC	120 * 200	Monotonic	–	–	–
BS0	120 * 200	Monotonic	40	–	–
BS1	120 * 200	Monotonic	40	1 D6	0.60
BS2	120 * 200	Monotonic	40	2 D6	1.20
BS3	120 * 200	Monotonic	40	3 D6	1.80
BRC	120 * 200	Repeated	–	–	–
BR0	120 * 200	Repeated	40	–	–
BR1	120 * 200	Repeated	40	1 D6	0.60
BR2	120 * 200	Repeated	40	2 D6	1.20
BR3	120 * 200	Repeated	40	3 D6	1.80

index should exceed this minimum value to prevent the occurrence of sudden failure in the strengthened flexural members. The curvature ductility indexes (μ_{ϕ}) of all the UHP-SHCC-strengthened beams are lower than the value obtained for the control beam, as shown in Table 5. However, the curvature ductility index (μ_{ϕ}) of beams BS1, BS2 and BS3, strengthened with steel reinforced UHP-SHCC layer, are higher than the one obtained for beam BS0, strengthened with unreinforced UHP-SHCC layer that because of the strain localization occurred in the unreinforced strengthening layer which made a rapid collapse. The results seem to indicate that the use of steel reinforcement can successfully enhance the ductility of UHP-SHCC strengthened beams. Moreover, 0.6%, 1.2% and 1.8% steel reinforcement enabled beams BS1, BS2 and BS3 to attain a curvature ductility index (μ_{ϕ}) of 2.09, 3.70 and 3.72 respectively, which, according to (FIB, 1990) recommendations, is adequate to guarantee satisfactory ductility.

3.5. Toughness and dissipated energy

Toughness was measured as the area under the load – deflection curve up to the peak for beams subjected to static load (group I). While energy dissipation is a relevant parameter in order to analyze the performance of reinforced concrete member subjected to repeated loading (group II), [19]. For group (I), the toughness was measured as explained before, which may be considered also as a ductility indicator. As shown in Table 5, the toughness of all the UHP-SHCC strengthened beams are lower than the value obtained for the control beam. However, the toughness of beams BS1, BS2, and BS3, strengthened with steel reinforced UHP-SHCC layer, are higher than the one obtained for beam BS0, strengthened with unreinforced UHP-SHCC layer. The results seem to indicate that the use of steel reinforcement can successfully enhance the ductility of UHP-SHCC strengthened beams. Moreover, 1.8% steel reinforcement enabled beam BS3 to attain a toughness of (2283), which is closer to other one (2088) obtained by 1.2% steel reinforcement beam BS2.

For group (II), Energy dissipation was measured and listed in Table 6. For structures, surviving a seismic event depends mainly on their capacity for energy dissipation. Greater the energy dissipated, better the specimen performance. The injected energy into the structure has two forms: dissipated energy (ABCDA); and recoverable energy (ADCEA) as shown in Fig. 10 of a typical loading cycle. Total energy absorbed by the system is the sum of dissipated energy and recoverable energy [1]. The dissipated energy is the

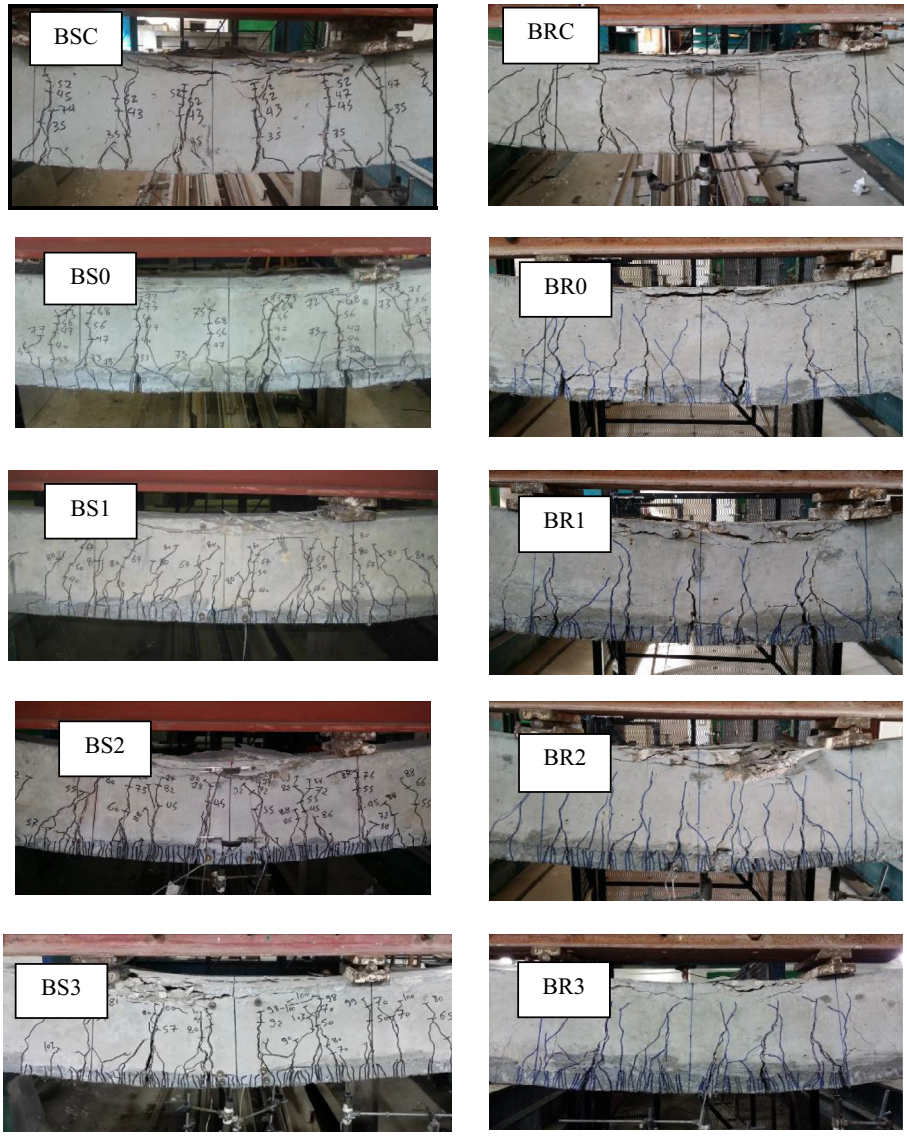


Fig. 6. Cracks pattern and failure mode of tested beams.

Table 4
Test results for all specimens in groups (I) and (II).

Group Name	Specimen Code	Cracking				Yield		Ultimate		Cracks developed in the UHP-SHCC layer		
		Substrate concrete		UHP-SHCC		Main reinforcement						
		Load (kN)	Deflection (mm)	Load (kN)	Deflection (mm)	Load (kN)	Deflection (mm)	Load (kN)	Deflection (mm)	S_{av} (mm)	S_{max} (mm)	N
Group (I)	BSC	15.2	1.72	-	-	41.4	6.90	53.4	50.84	-	-	-
	BS0	31.4	0.93	46.6	1.39	73.4	7.10	77.0	9.62	29.4	105	22
	BS1	32.0	0.79	46.2	1.20	81.6	7.55	84.0	11.44	14.3	50	46
	BS2	32.2	0.73	46.9	1.16	90.2	7.80	94.0	23.60	9.3	27	66
	BS3	32.9	0.72	47.0	1.18	95.4	8.05	103.7	26.13	9.1	25	69
Group (II)	BRC	–	–	–	–	40.2	7.03	49.7	56.50	–	–	–
	BR0	–	–	–	–	71.3	7.25	71.0	18.03	25.6	95	26
	BR1	–	–	–	–	79.6	7.76	79.0	22.01	12.9	45	51
	BR2	–	–	–	–	89.5	7.94	91.0	26.02	8.3	23	72
	BR3	–	–	–	–	95.1	8.26	100.0	28.07	8.2	23	74

area enclosed by the hysteresis loop as shown in Fig. 10 and represents the structural element capacity to mitigate the repeated loading effect, which causes excessive cracking and permanent deformation. In UHP-SHCC strengthening layer, fibers inside the matrix also act as energy dissipater because inelastic behavior due to fiber deformation, fiber slip and fiber breaking or pulling out are also main factors along with inelastic behavior of steel bars and cracking of concrete to dissipate major part of the injected

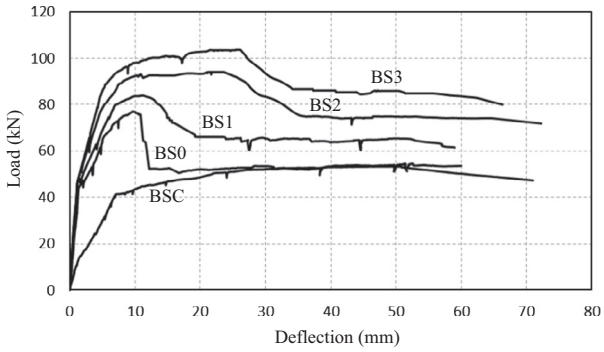


Fig. 7. Load-deflection relationships for group (I).

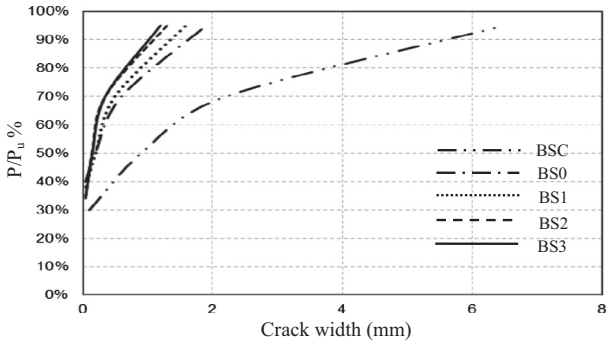


Fig. 9. load-crack width relationship for group (I).

energy into the structures during seismic excitation or repeated loads.

The energy dissipated during each loading cycle was calculated using the trapezoidal rule to determine the area within the load-deflection hysteresis loop. The value of dissipated energy in all cycles at same loading stage was determined. The values of dissipated energy (ABCDA) of each type of beam are given in Table 6 and are graphically shown in Fig. 11. In Fig. 11, it can be observed that, during first three loading stages, for all beams the dissipated energy increased by increasing reinforcement ratio used in the

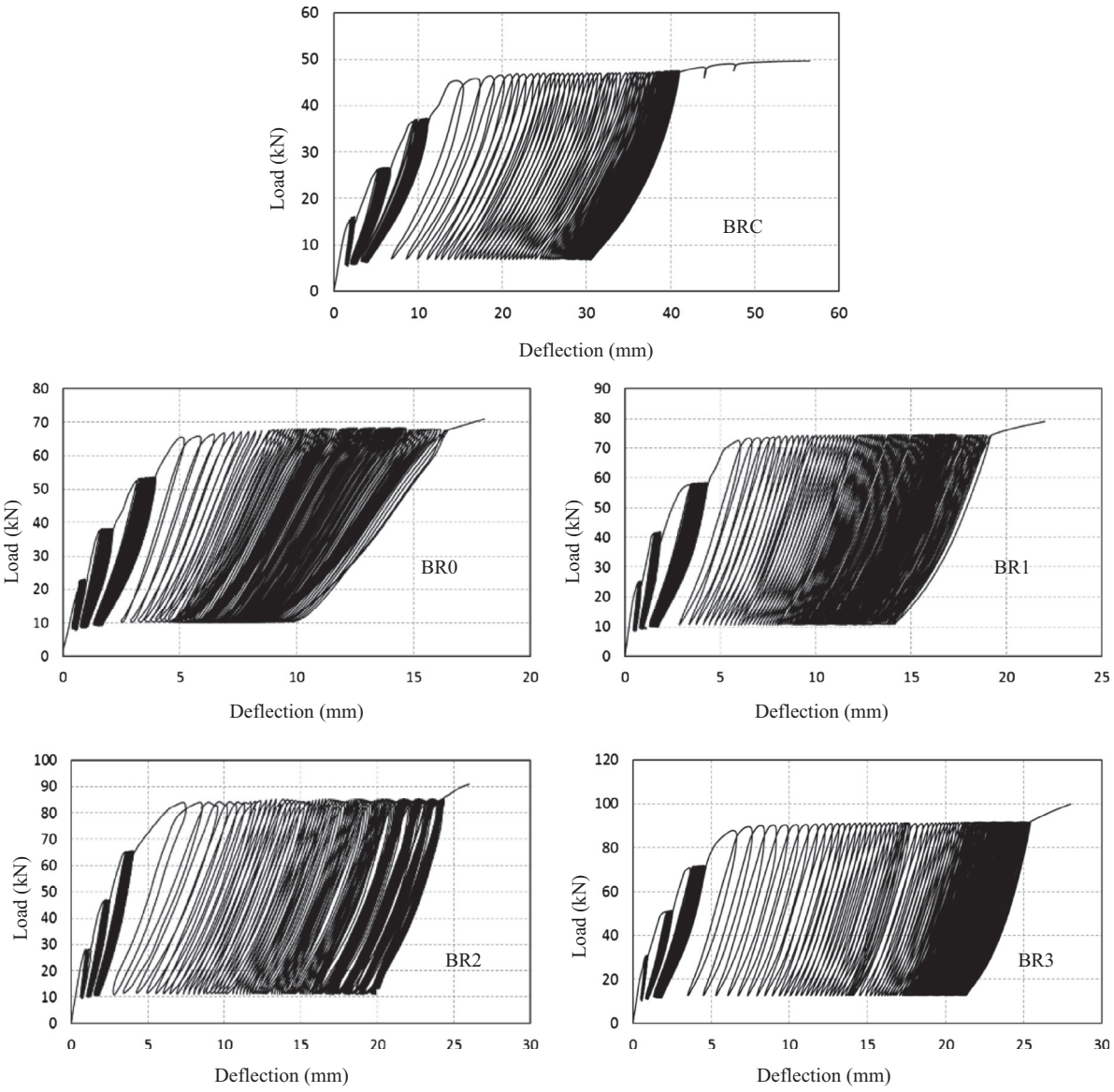


Fig. 8. Load-deflection relationships for group (II).

Table 5
Ductility index and toughness for group (I).

Beam	Yield curvature (km^{-1})	Ultimate curvature (km^{-1})	Ductility index ($\mu_{\emptyset}$)	Toughness (kN mm)
BSC	18.75	143.11	7.63	2360
BS0	19.38	23.75	1.22	745
BS1	19.13	40.00	2.09	1032
BS2	19.81	73.25	3.70	2088
BS3	19.94	74.25	3.72	2283

Table 6
Dissipated energy (kN.mm) for beams in group (II).

Beam	Loading stages				Total
	10–30%	10–50%	10–70%	10–90%	
BRC	82	609	1663	4224	6578
BR_0	55	283	694	2352	3384
BR_1	60	316	850	4385	5611
BR_2	62	392	1052	5503	7009
BR_3	65	447	1243	5960	7715

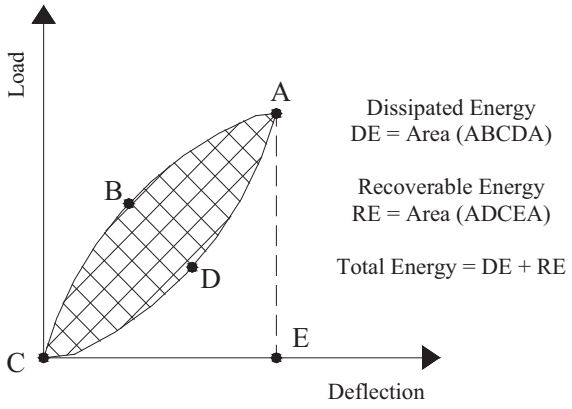


Fig. 10. Typical loading cycle for a structural element.

strengthening layer, however still smaller than the control beam, that enhancement in energy dissipated occurred in strengthened beams was due to fibers inside the matrix of UHP-SHCC layer and the additional steel bars used in this layer, which act as energy dissipaters [11], but still smaller than the control beam which was able to made large deflection and lead to widely cracks compared to other strengthened beams at the same load stage that helps to dissipate more energy.

During the fourth stage (10–90%), it can be observed that all strengthened beams with additional reinforcement in UHP-SHCC layer (BR3, BR2 and BR1) were able to dissipated more energy than the control beam and beam BR0, this is because that the great contribution gained from the fibers and additional reinforcement in the strengthening layer, which obtained larger strain in the UHP-SHCC layer than other strengthened beams and this large strain gained large dissipated energy. However beam BR0, with no additional reinforcement in UHP-SHCC layer, had rapidly localized failure of the strengthening layer due to high strain concentration points in the strengthening layer produced by the cracks developed in the concrete substrate. In generally, Table 6 lists the total dissipated energy obtained by beams during all loading stages, it can be seen that maximum gain registered in the total energy dissipation by beams BR3, BR2 and BR1 compared to beam BR0 is 130%, 107% and 66%, respectively.

It is important to know that, from the observation of the hysteresis loops, the energy dissipated in the first cycles of each load

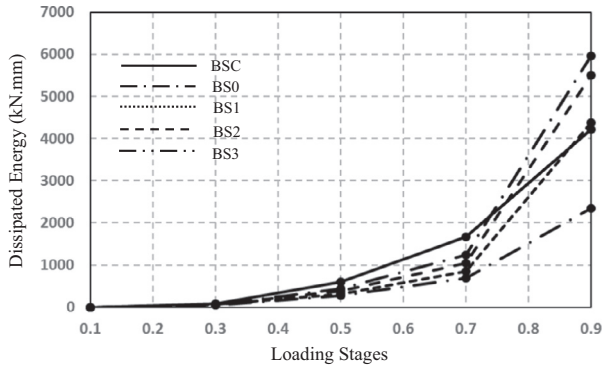


Fig. 11. Dissipated energy for beams in group (II).

level was greater than in the subsequent cycles. This is because that the crack development, widening or propagation occurred in the first cycles while, in the subsequent cycles, the cracks marginally extended in their length but open and close in alternate loading. The possible explanation of greater value of dissipated energy in the first cycles of loading is that when deflection is increased, crack is extended and the fibers present in the path of the crack resist their propagation causing much energy dissipation. Due to high stress level occurred suddenly in the first cycles, the fibers break during that cycles and no more or little damage of fibers occur in subsequent cycles of loading at the same load value.

3.6. Stiffness degradation

In the case of reinforced concrete beam, stiffness gets reduced when the beam is subjected to cyclic/repeated/dynamic loading. This reduction in stiffness is due to the following reasons: during repeated loading, the materials, viz. concrete and steel, are subjected to loading, unloading, and reloading processes. This will cause initiation of micro-cracks inside the beam and will sometimes lead to the low fatigue limit of the materials. This, in turn, increases the deformations of the beam, thus resulting in increasing the damage level of the beam, which lead to reduction in the stiffness. Hence, it is necessary to evaluate degradation of stiffness in the beam subjected to repeated loading.

In order to determine the degradation of stiffness, the following procedure was adopted. A line 1–2 joining the low and the peak loads of the first cycle, as shown in Fig. 12, is drawn. The slope of this line is known as the secant stiffness [18]. Similarly, from the slope of the line joining the points 3 and 4 of the second cycle, secant stiffness of the second cycle is obtained. Similar procedure was adopted for all the other cycles. The values of the secant stiffness obtained for each cycle are plotted for all the specimens, and the plots are given in Fig. 13.

During each stage of loading, from Fig. 13 it can be noticed the same behavior of all beams, that the beams started the first stage with its highest stiffness and during the first ten cycles it can be noticed small degradation in the stiffness, due to the sequent damage occurred in the beams from loading and unloading. Then when the damage level of beams be constant the degradation noticed to be insignificant up to the end of this stage, however it can be noticed the great degradation occurred in the fourth stage of loading during the first-twenty-five cycles in all specimen as the beams were close to failure and the main reinforcement was reached its yield strength. However, beam BR0, which has no additional reinforcement in the strengthening layer, has a different behavior in the fourth stage it was noticed the severe degradation occurred along all cycles in the fourth stage of loading that may be due to increasing the damage level of beam under repeated loading,

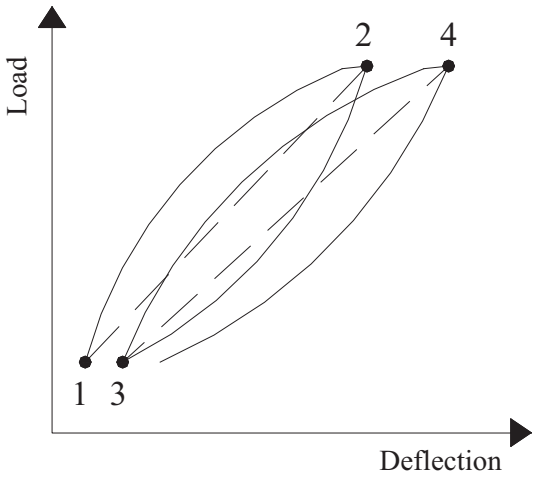


Fig. 12. The procedure adopted for determining secant stiffness.

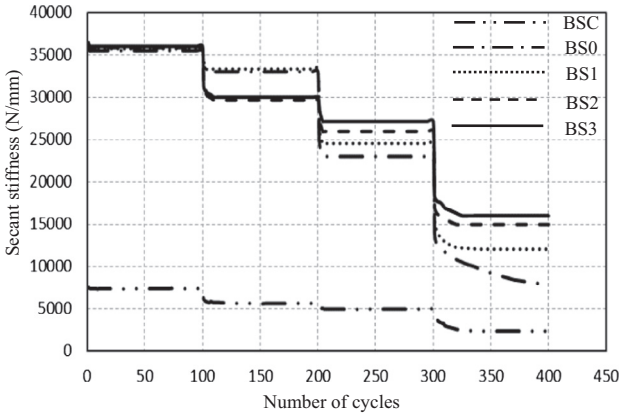


Fig. 13. Relation between secant stiffness and number of cycles.

which induced by the localized failure occurred in the strengthening layer produced by the high strain concentration points in the UHP-SHCC strengthening layer from the cracks developed in the concrete substrate, that emphasized the effect of additional reinforcement used in the strengthening layer, therefore we resolved to study the effect of applying higher number of cycles to get the high fatigue response in the future work.

In generally, it may be noted from Fig. 13 that all strengthened beams have stiffness higher than control one in all loading stages. It may also be noted from this figure that the increase of reinforcement ratio used in the strengthening layer leads to increase in stiffness in all loading stages, however this increase considered insignificant during the first stage that may be attributed to the fact that at the first stage, cracks would not have propagated and hence the fibers in the strengthening layer were not effective in the absence of formation of cracks. As the number of cycles increased and second stages started, micro-cracks developed, and fibers, which are distributed at random, intercept these cracks and bridge across these cracks. This action will control further propagation of cracks and will result in higher energy demand for breaking and pull-out of fibers in the vicinity of cracks. During this process, stiffness of the beam with reinforced strengthening layer will not undergo much reduction when compared to that without reinforcement in the strengthening layer. It is important to explain the unexpected behavior of beams BR2 and BR3, which have lower stiffness than other strengthened beams only in the second stage of loading, that because of cracking of beams BR2 and BR3 was occurred in this stage in contrary of beams BR0 and BR1 which cracking was occurred in the third stage of loading companion to larger degradation in the stiffness.

3.7. Repeatability and permanency

Two indicators usually used to analyze the behavior of a tested beam under repeated loading are the following and all are related to the response of the beam in terms of displacement (ACI 437R-03, 2003):

- Repeatability: It represents the behavior of the beam during two sequent identical loading cycles and by measuring the repeatability of deflections, which is the ratio of the difference between the maximum and residual deflection recorded during the second cycle to that of the first, one is not only monitoring the beam's behavior, but also gaining assurance that the data collected during the test are consistent. It is calculated according to the following equation referring to Fig. 14:

$$\text{Repeatability} = \frac{\Delta B_{max} - \Delta B_r}{\Delta A_{max} - \Delta A_r} \times 100\% \quad (1)$$

where;

ΔB_{max} = maximum deflection in Cycle B under a load of P max
ΔB_r = residual deflection after Cycle B under a load of P min
ΔA_{max} = maximum deflection in Cycle A under a load of P max
ΔA_r = residual deflection after Cycle A under a load of P min
P_{max} = maximum test load for one cycle
P_{min} = minimum test load for one cycle

The previous equation was verified for all two sequent cycles as shown in Fig. 15. As the more consistent the collected data during any two identical cycles, the more confidence in the instrumentation's adequacy, for all beams, the repeatability values were greater than the lower acceptance limit of 95% and less than the upper limit of 120% (ACI 437R-03, 2003). This increases the confidence in the accuracy of the used instrumentation.

- Permanency: It is the relative value of the residual deflection to the maximum deflection during the second load cycle of each load set and represents the amount of permanent change displayed by any structural response parameter during the second of two identical load cycles. It is computed by the following equation referring to Fig. 14 (for example, during cycle B):

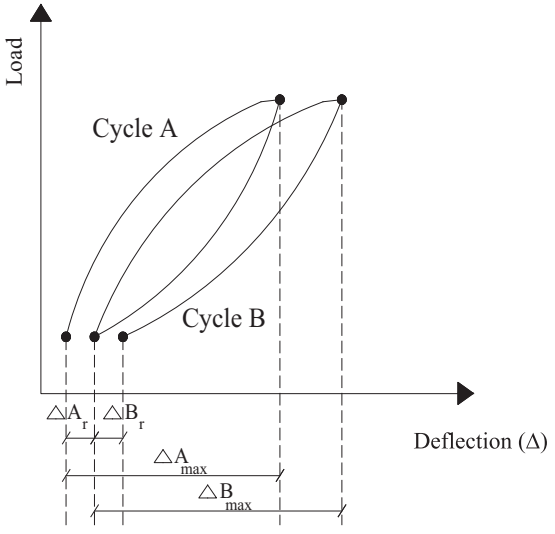


Fig. 14. Schematic load versus deflection curve for two cycles.

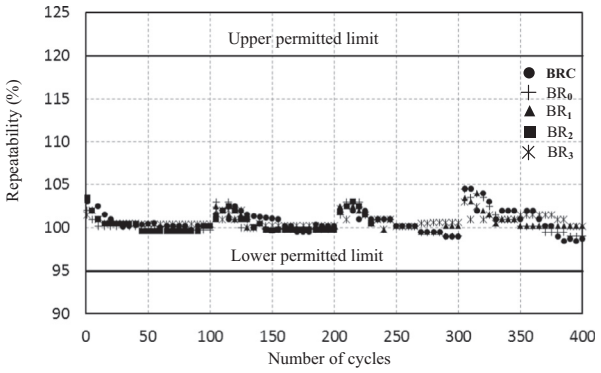


Fig. 15. Relation between repeatability and number of cycles.

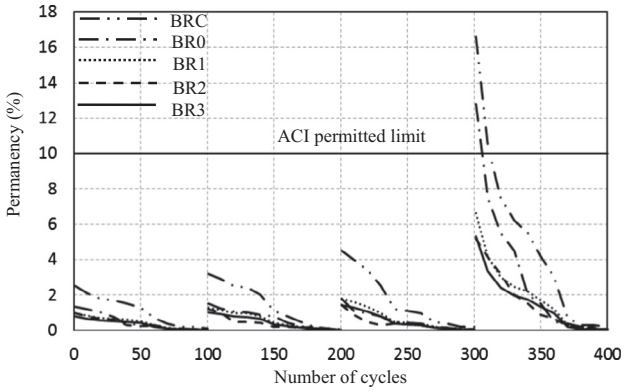


Fig. 16. Relation between permanency and number of cycles.

$$\text{Permanency} = \frac{\Delta B_r}{\Delta B_{\max}} \times 100\% \quad (2)$$

The evaluation criterion is that a deflection permanency of less than 10% is acceptable (ACI 437R-03, 2003). Therefore, from Fig. 16, it can be noticed that during each stage of loading as the number of cycles increased, the permanency level decreased that because of the relatively great damage occurred during the first cycles at each stage of loading that appears in the permanent deflection in the hysteresis loops, which was larger in the first cycles compared to the last cycles at each stage of loading, the strengthened beams had lower permanency level than control one that expressed relatively low damage level occurred in the strengthened beams. As shown in Fig. 16 all permanency levels for all strengthened beams are not exceeded the permitted level according to (ACI 437R-03, 2003), however beam BR0 and the control beam BRC, in the first few cycles of the fourth stage, were exceeded the permitted level aforementioned 10%, it may be an indication that the repeated loading had a significant damaging effect on the two beams at this stage of loading.

4. Analytical study for static loading

This section is a trial to estimate flexural capacity of RC beams strengthened with strain hardening cementitious composites. The adopted theoretical approach is verified by comparison with the experimental results. Designing structural members using ultimate limit state concept is based on the following assumptions: Linear strain distribution is assumed. This is based on Bernoulli's hypothesis that plane sections before bending remain plane and perpendicular to the neutral axis after bending, tensile strength of concrete is neglected (This assumption is made for simplification. Since, in fact, concrete resist tension before cracking and after cracking in segments between cracks), full composite action between UHP-SHCC layer and embedded additional reinforcement and Perfect bond exists between UHP-SHCC layer and the surrounding concrete.

General equation for the calculation of nominal flexural strength of beam sections with FRP external reinforcement in simple beams with tension steel only is presented by (ACI 440.2R-02, 2005) as the following:

$$M_n = A_s f_s \left(d_s - \frac{\lambda c}{2}\right) + \psi_f A_f f_{fe} \left(d_f - \frac{\lambda c}{2}\right) \quad (3)$$

For beams strengthened with UHP-SHCC layer, (ACI 440.2R-02, 2005) equations are adopted and modified to take into considerations the effect of secondary steel, UHPSHCC layer and embedded additional reinforcement. General scheme for the internal strain and stress of a rectangular section according to the proposed format may be drawn considering the equilibrium of the section under the forces as shown in Fig. 17.

The equilibrium equation of the section

$$C_c + C'_s = T_s + T_{UHP} + T_{add} \quad (4)$$

The nominal moment of the section is calculated by the following equation

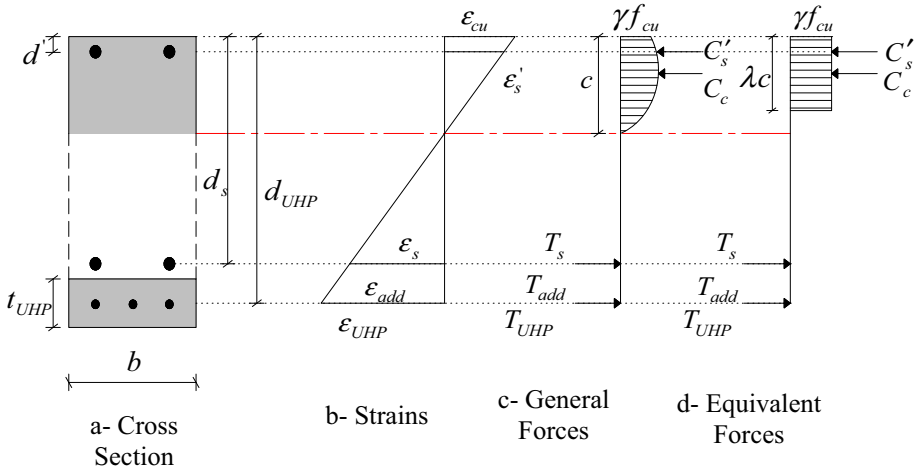


Fig. 17. Stress-strain relationship for RC beams.

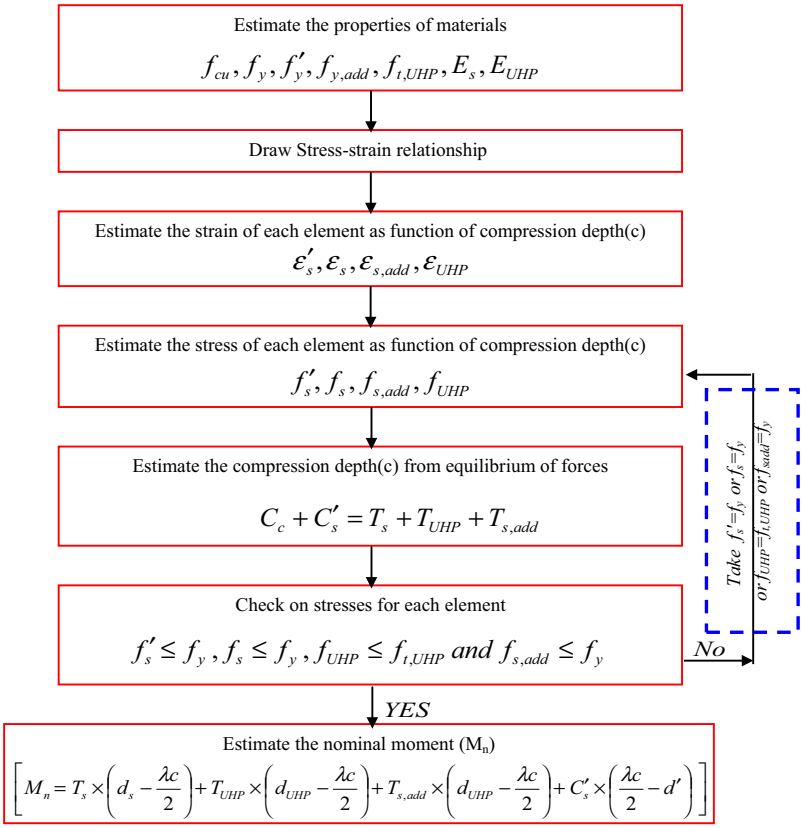


Fig. 18. Nominal moment calculation flow chart.

Table 7
Verification of proposed model and experimental results for group (I).

Specimen	$M_{n,experimental}$ kN m	$M_{n,proposed}$ kN m	$\frac{M_{n,experimental}}{M_{n,proposed}}$
BSC	12.02	10.93	1.09
BS0	17.33	17.18	1.02
BS1	18.90	18.79	1.01
BS2	21.15	20.38	1.04
BS3	23.33	21.95	1.06
Average			1.05

$$M_n = T_s \times \left(d_s - \frac{\lambda_c}{2}\right) + T_{UHP} \times \left(d_{UHP} - \frac{\lambda_c}{2}\right) + T_{s,add} \times \left(d_{UHP} - \frac{\lambda_c}{2}\right) + C'_s \times \left(\frac{\lambda_c}{2} - d'\right) \quad (5)$$

where:

$$C_c = \gamma \times f_{cu} \times b \times \lambda_c \quad (6)$$

$$C'_s = As\prime \times f'_s = As\prime \times E_s \varepsilon_{cu} \frac{c - d'}{c} \quad (7)$$

$$T_s = A_s \times f_s = A_s \times E_s \varepsilon_{cu} \frac{d_s - c}{c} \quad (8)$$

$$T_{UHP} = A_{UHP} \times f_{UHP} = b\, t_{UHP} \times E_{UHP}\, \varepsilon_{cu} \frac{d_{UHP} - c}{c} \quad (9)$$

$$T_{s,add} = A_{s,add} \times f_{s,add} = A_{s,add} \times E_s \varepsilon_{cu} \frac{d_{UHP} - c}{c} \quad (10)$$

The flexural nominal moment predictions based on the analytical model are summarized in flowchart in Fig. 18. The proposed equation was adopted for different beams strengthened and tested experimentally up to failure; Table 7 shows the values of nominal moment for all beams in group (I) that was calculated by using proposed equation ($M_{n,proposed}$) and the experimental capacity results ($M_{n,experimental}$). From Table 7, it can be concluded that the adopted analytical model succeeded to predict the nominal capacity as close as possible to the experimental investigation.

5. Conclusions

Based on the results obtained in this work, the following conclusions can be drawn:

- UHP-SHCC has good bonding with substrate concrete under repeated loading as there is no delamination occurred which is similar to fact well known in static load.
- Great damage level was observed in the stiffness for beams strengthened with unreinforced UHP-SHCC layer under repeated load.
- The load-deflection hysteresis loops indicate the capability of the small amount of steel reinforcement to reduce the stiffness degradation of the UHP-SHCC strengthening layer under repeated loading.
- The convergent previous results of cracks number, ductility index, toughness and energy dissipated for beams strengthened with 1.2% and 1.8% reinforcement ratio in the strengthening layer emphasized the insignificant use of reinforcement ratio higher than 1.2% in the ductility enhancement of the strengthened beams in the similar conditions used in the experimental tests.

- Increasing the reinforcement ratio embedded in the UHP-SHCC strengthening layer lead to increasing the total dissipated energy of the specimens subjected to repeated load.
- The adopted theoretical model gave very accurate prediction of the nominal moment for beams strengthened with UHP-SHCC layer subjected to static load.

Acknowledgements

The tests were carried out in the Reinforced Concrete Laboratory, Faculty of Engineering, Tanta University, Egypt. The authors are grateful for the precious technical assistance of lab staff. This work is a part of master thesis of the fourth author.

References

[1] Abdelsamine S, Tom B. Hysteresis energy and damping capacity of flexural elements constructed with different concrete strengths. Eng Struct 2010;32:297–305.
[2] ACI 318M–14. (2014): Building Code Requirements for structural concrete and commentary (ACI 318RM-14).
[3] Amino T, Tanaka R, Habuchi T, Kunieda M, Iwanami M. Steel corrosion protective performance of UHP-SHCC with multiple fine cracks under bending. Tokyo, Japan: Life-Cycle Civil Engineering (IALCCE); 2015. p. 1703–8.
[5] Hussein H, Kunieda M, Nakamura H. Strength and ductility of RC beams strengthened with steel-reinforced strain hardening cementitious composites. J Cem Concr Compos 2012;34(9):1061–6.
[6] JCI-DFRCC committee. DFRCC terminology and application concepts. J Adv Concr Technol 2003;1(3):335–40.
[7] Kamal A, Kunieda M, Ueda N, Nakamura H. Evaluation of crack opening performance of a repair material with strain hardening behavior. J Cem Concr Compos 2008;30(10):863–71.
[8] Kunieda M. Hybrid surface protection repair system using UHP-SHCC for concrete structures. In: Concrete solutions international conference. p. 399–402.
[9] Kunieda M, Choonghyun K, Ueda N, Nakamura H. Recovery of protective performance of cracked ultra high performance-strain hardening cementitious composites (UHP-SHCC) due to autogenous healing. J Adv Concr Technol 2012;10(9):313–22.
[10] Kunieda M, Hussein M, Ueda N, Nakamura H. Fracture behavior of steel reinforced UHP-SHCC under axial tension, Fracture mechanics of concrete structures. Proceedings FRAMCOS-7; 2010. p. 1557–1564.
[11] Daniel L, Loukili A. Behavior of high strength fiber-reinforced concrete beams under cyclic loading. ACI Struct J 2002;99(3):248–56.
[12] Li VC. From micromechanics to structural engineering – the design of cementitious composites for civil engineering applications. Struct Eng/Earthquake Eng, JSCE 1993;10(2):37–48.
[13] Li VC. Engineered cementitious composites – tailored composites through micromechanical modeling. In: Banthia N, Bentur A, Mufti A, editors. Fiber-reinforced concrete: present and the future. Montreal: Canadian society for civil engineering; 1998. p. 64–97.
[14] Li VC, Kanda T. Engineered cementitious composites for structural applications. ASCE J Mater Civil Eng 1998;10(2):66–9.
[15] Li VC. ECC for repair and retrofit in concrete structures. In: Fracture mechanics of concrete structures, proceedings FRAMCOS-3. Freiburg (Germany): Aedification Publishers; 1998. p. 1715–26.
[16] Li VC. On engineered cementitious composites (ECC)-a review of the material and its applications. J Adv Concr Technol 2003;1(3):215–30.
[17] Naaman AE. Strain hardening and deflection hardening fiber-reinforced cement composites. In: Naaman AE, Reinhardt HW, editors. High performance fiber-reinforced cement composites (HPFRCC4), Proceedings of the fourth international RILEM workshop. p. 95–113.
[18] Shannag MJ, Abu-Dyya N, Abu-Farsakh G. Lateral load response of high performance fiber-reinforced concrete beam-column joints. Constr Build Mater 2005;19(7):500–8.
[19] Verderame GM et al. Seismic response of RC columns with smooth reinforcement Part II: cyclic tests. Eng Struct 2008;30:2289–300.